JOURNAL OF CHEMICAL & ENGINEERING DATA

ARTICLE

pubs.acs.org/jced

Enhanced Cationic Dyes Removal from Aqueous Solution by Oxalic Acid Modified Rice Husk

Weihua Zou,*,† Ke Li,† Hongjuan Bai,† Xiaolan Shi,† and Runping Han*,‡

†School of Chemical Engineering and Energy, Zhengzhou University, #100 Kexue Road, Zhengzhou, 450001, P. R. China

‡Department of Chemistry, Zhengzhou University, #100 Kexue Road, Zhengzhou 450001, P. R. China

ABSTRACT: The adsorption of two basic dyes, namely, methylene blue (MB) and malachite green (MG), onto natural rice husk (NRH) and oxalic acid modified rice husk (MRH) was studied in a batch adsorption system. Factors influencing dyes adsorption such as the concentration of the adsorbate, the pH, the salt concentration, the temperature, and the contact time were investigated. The Langmuir and Freundich isotherms were used to fit the equilibrium data, and the results showed that the Langmuir isotherm exhibited a little better fit to the MG adsorption data by both adsorbents, while the Freundlich isotherm seemed to agree better with the MB adsorption. The kinetic experimental data were analyzed using three kinetic equations, via the pseudo-first-order equation, the pseudo-second-order equation, and the intraparticle diffusion model, to examine the mechanism of adsorption and the potential rate-controlling step. The mechanism of the process was found to be complex, consisting of both surface adsorption and pore diffusion. The values of the effective diffusion parameter, D_i, were estimated to be of the order of 10^{-8} $cm^2 \cdot s^{-1}$, indicating that the intraparticle diffusion was not the rate-controlling step. Calculated thermodynamic parameters showed that the adsorption of MB and MG onto MRH was feasible, spontaneous, and endothermic. The removal capacities of NRH and MRH adsorbing dyes from aqueous solution were compared. By functionalizing, the adsorption capacity (q_e) of rice husk for MB or MG was increased from (19.77 to 53.21) $mg \cdot g^{-1}$ or (28.00 to 54.02) $mg \cdot g^{-1}$ at 293 K, respectively. The carboxyl groups on the surface of the MRH were primarily responsible for the sorption of dyes. It is suggested that MRH may be suitable as an adsorbent material for adsorbing MB and MG from aqueous solutions.

1. INTRODUCTION

Dyes are present in different concentrations in wastewaters of industries such as plastic, textile, dye, dyestuffs, and so forth.[1] These dyes color the water, making penetration of sunlight to the lower layers impossible and thus affecting the process of photosynthesis. It is, therefore, very important to remove these dyes from the water.[2] Adsorption techniques have proved to be an effective and attractive process for removal of nonbiodegradable pollutants (including dyes) from wastewater.[3,4] The most widely used adsorbent for the removal of dyes is activated carbon, which is expensive and has a high regeneration cost.[5,6] Therefore, interest is growing to find alternatives to carbon adsorbents. Recently, attention has been focused on the development of low-cost adsorbents for applications concerning the treatment of wastewater.[4,7] Agricultural byproducts such as peanut husk,[8] apple pomace and wheat straw,[9] wheat shell,[10] cereal chaff,[11] fruit peel,[12] bark,[9] and leaves[13] have been widely studied for dye removal from wastewater. Generally, the sorption capacities of crude agricultural byproduct are low. For improving the sorption capacity of crude agricultural byproduct, chemical modification was used.[14−17] However, there are few studies on the research of cation dye adsorption onto an oxalic acid modified agricultural byproduct, such as rice husk.

Rice husk is an agricultural waste and a byproduct of the rice milling industry estimated to be more than 100 million tonnes, 96 % of which is generated in developing countries. The utilization of this source of agricultural waste would both solve a disposal problem as well as give access to a cheaper material for adsorption in water pollutant control systems.

In this work, several batch experiments were performed on natural rice husk (NRH) and oxalic acid modified rice husk (MRH) toward aqueous solutions of methylene blue (MB) and malachite green (MG). Further, the kinetics and the mechanistic steps involved in the sorption process were evaluated at different initial MB or MG concentrations. The adsorption capacity of the adsorbents used in the present work was also compared with other adsorbents used by different researchers.

2. MATERIALS AND METHODS

2.1. Preparation of MRH. Fresh rice husk biomass was collected from farmland in Zhengzhou City, P. R. China. This husk was washed several times with distilled water and then dried at 60 °C for 8 h in an oven. The dry rice husk was crushed to a powder and sieved to provide (0.850 to 0.425) mm fractions for chemical modification.

Rice husk modified with oxalic acid (MRH) was prepared according to the modified method of Vaughan et al.[18] NRH was mixed with a 0.6 $mol \cdot L^{-1}$ solution of oxalic acid (OA) at a ratio of 1:12 (rice husk with acid, w/v) and stirred for 30 min at 20 °C. The acid rice husk was placed in a stainless steel tray and dried for 24 h at 50 °C in a forced air oven. Thermochemical esterification between acid and rice husk was effected by raising the oven temperature to 120 °C for 90 min. After cooling, the esterified rice husk was washed with distilled water until the wash liquid

Received: August 31, 2010
Accepted: March 7, 2011
Published: March 22, 2011

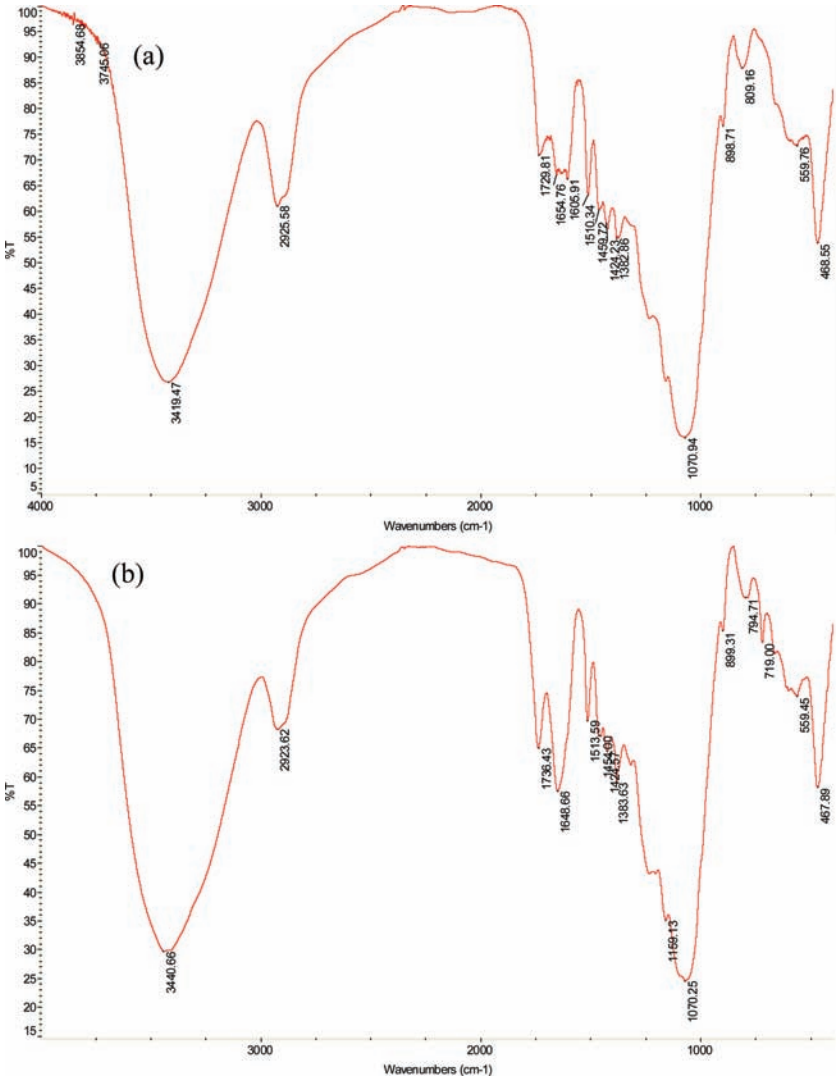

Figure 1. Fourier transform infrared spectra of (a) NRH and (b) MRH.

exhibited no turbidity when 0.1 mol·L^{-1} $CaCl_2$ was added. After filtration, MRH was suspended in 0.1 mol·L^{-1} NaOH solution at a suitable ratio and stirred for 60 min, followed by washing thoroughly with distilled water to remove residual alkali and then dried at 50 °C for 24 h and preserved in a desiccator for subsequent use.

The chemical modification of rice husk may be expressed schematically as:

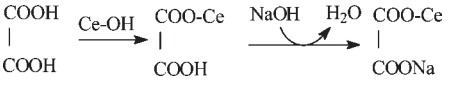

where Ce−OH corresponds to NRH.

2.2. Preparation of Dye Solutions. All chemicals and reagents used for experiments and analyses were of analytical reagent grade. The MB or MG stock solution of 500 mg·L^{-1} concentration was prepared by dissolving an accurately weighed amount of MB and MG in distilled water. The experimental solutions were obtained by diluting the dye stock solutions in accurate proportions to obtain different initial concentrations.

2.3. Experimental Methods and Measurements. Equilibrium adsorption studies were undertaken by batch methods at (293, 303, and 313) K. A series of 50 mL conical flasks were used for such studies, with each flask containing MRH or NRH at a mass loading of 3 g·L^{-1} in the presence of 10 mL of an MB or MG solution at an initial concentration within the range (20 to 450) mg·L^{-1}. The conical flasks were agitated on an orbital shaker at 120 rpm for 480 min with samples of the solutions being removed for dye analysis after equilibrium had been attained. The effect of pH on adsorption of MB or MG onto both adsorbents was investigated by varying the initial solution pH from (2.0 to 10.00). The effect of the ionic strength on dye uptake was examined using KCl or $CaCl_2$ solutions to adjust the ionic strength.

Kinetic experiments were carried out by loading 3 g·L^{-1} NRH or MRH in several sets of conical flasks containing 10 mL of dye solution of known initial concentration. The flasks were then subjected to agitation using water bath shakers for different contact time intervals. Flasks were taken from the shakers at regular time intervals, and the remaining concentration of MB and MG in solution was estimated.

After adsorption, the adsorbent was separated by filtering, and the concentration of dyes in solution was performed on a UV−vis-3000 spectrophotometer (Shimadzu Brand UV-3000) at 660 nm for MB and 620 nm for MG.

dx.doi.org/10.1021/je100893h |*J. Chem. Eng. Data* 2011, 56, 1882–1891

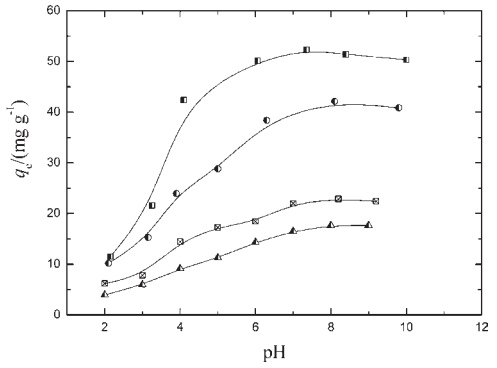

Figure 2. Effect of the initial solution pH on the removal of MB and MG by both adsorbents (initial dye concentration 250 mg·L^{-1}, NRH or MRH dosage 3 g·L^{-1}, contact time 480 min, 283 K). ◧, MB (MRH); ▲, MB (NRH); ◐, MG (MRH); □ with ×, MG (NRH).

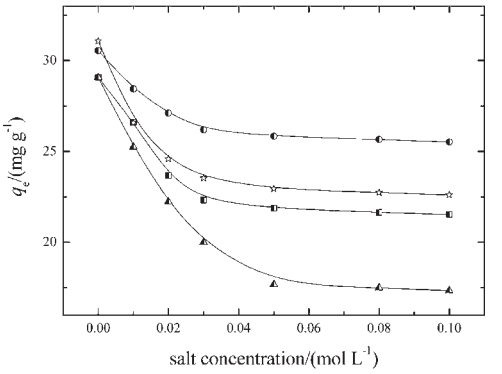

Figure 3. Effect of KCl and $CaCl_2$ concentration on adsorption (initial dye concentration 100 mg·L^{-1}, MRH dosage 3 g·L^{-1}, contact time 480 min, 283 K). ◧, MB (KCl); ▲, MB ($CaCl_2$); ◐, MG (KCl); ☆, MG ($CaCl_2$).

The amount of dye adsorbed per unit weight of adsorbent (q) was calculated using the following equation:

$$q = \frac{V(C_0 - C)}{1000m} \quad (1)$$

where V (L) is the volume of the solution, C_0 (mg·L^{-1}) is the initial dye concentration, C (mg·L^{-1}) is the dye concentration at any time t, and m (g) is the dry weight of adsorbent employed.

3. RESULTS AND DISCUSSION

3.1. FTIR Spectra of NRH and MRH. Like all vegetable biomass, rice husk consists of abundant amounts of fiber- and protein-containing groups such as carboxyl, hydroxyl, amidogen, and so forth.[19] It would thus appear to be a good candidate for modification with carboxylic acids, with the addition of carboxyl functional groups possibly enhancing the sorption capacities of the rice husk. Figure 1 shows the corresponding IR spectra of NRH and MRH. As shown in Figure 1, the spectra displayed a number of absorption peaks, indicating the complex nature of the material. The broad absorption peaks at ca. 3419 cm^{-1} are indicative of the existence of bonded hydroxyl groups on the surface of the rice husk. This band was associated with the vibrations of the silanol group, the linked hydroxyl groups in cellulose and lignin, and adsorbed water on the husk surface. The peaks located at (1729 and 1654) cm^{-1} were characteristic of carbonyl group stretching from aldehydes and ketones.[20] These groups can be conjugated or nonconjugated to aromatic rings [(1640 and 1730) cm^{-1}, respectively]. The peak near 1424 cm^{-1} was also attributed to a stretch vibration of C−O from carboxyl groups. The strong C−O band at 1070 cm^{-1} also confirms the lignin structure of the rice husk.

From the Fourier transform infrared (FTIR) spectra of NRH and MRH, it was shown that the modification of the rice husk led to an increase in the adsorption band corresponding to the stretch vibration of the carboxyl group (at 1736 cm^{-1}), with the positions of some peaks being changed after modification. These results show that MRH possessed more carboxyl groups than NRH. These groups may function as proton donors, and as a consequence, deprotonated hydroxyl and carboxyl groups may be involved in coordination with positive dye ions. Dissolved MB or MG ions are positively charged and will undergo attraction on approaching the anionic MRH structure. On this basis, it is expected that MRH will show a strong sorption affinity toward MB and MG ions.

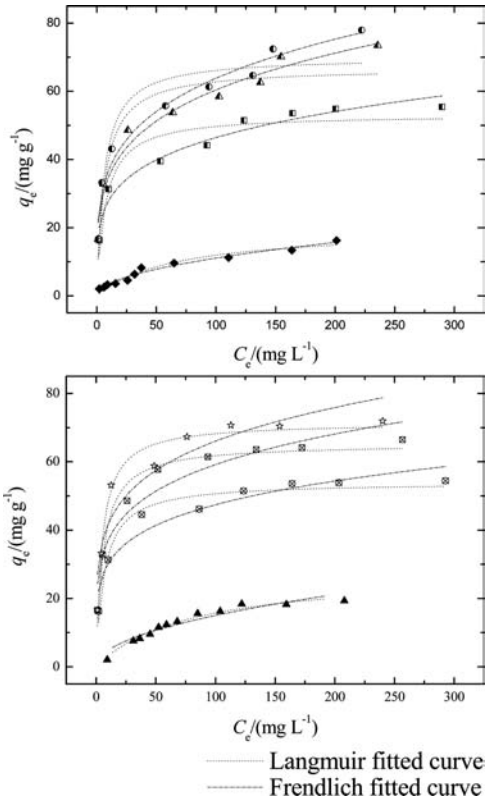

Figure 4. Equilibrium adsorption quantities of MB and MG adsorption at different equilibrium dye concentrations and predicted isotherm curves (NRH or MRH dose: 3 g·L^{-1}). ◧, MB (293 K); ▲, MB (303 K); ◐, MB (313 K); ♦, MB (293 K, NRH); ⊗, MG (293 K); □ with ×, MG (303 K); ☆, MG (313 K); ▲, MG (293 K, NRH).

3.2. Effect of Initial pH. It is well-known that the pH of a system is an important variable in the adsorption process. The pH of the dye solution affects not only the surface charge of the adsorbent, the degree of ionization of the materials, and the dissociation of functional groups on the active sites of the adsorbent, but also the structure of the dye molecule.[21] Figure 2 shows the effect of the initial solution pH on the amount of MB

Table 1. Langmuir and Freundlich Isotherm Constants for MB and MG Adsorption onto MRH or NRH at Different Temperatures Using Nonlinear Regressive Method

dye	model	T/K			
		293 (NRH)	293 (MRH)	303 (MRH)	313 (MRH)
MB	Langmuir				
	$K_L/(L\cdot mg^{-1})$	0.015 ± 0.003	0.140 ± 0.046	0.153 ± 0.053	0.166 ± 0.052
	$q_m/(mg\cdot g^{-1})$	19.77 ± 1.83	53.21 ± 2.43	66.90 ± 3.44	70.10 ± 3.63
	R^2	0.9578	0.9030	0.9091	0.9182
	χ^{2a}	4.749	3.641	6.313	6.152
	Freundlich				
	K_F	1.096 ± 0.174	16.87 ± 1.860	20.27 ± 1.86	21.26 ± 2.01
	$1/n$	0.502 ± 0.033	0.220 ± 0.023	0.237 ± 0.022	0.239 ± 0.020
	R^2	0.9746	0.9630	0.9719	0.9749
	χ^2	0.942	1.546	2.102	2.388
MG	Langmuir				
	$K_L/(L\cdot mg^{-1})$	0.022 ± 0.004	0.15 ± 0.025	0.177 ± 0.030	0.208 ± 0.031
	$q_m/(mg\cdot g^{-1})$	28.00 ± 1.62	54.02 ± 1.03	65.26 ± 1.65	71.49 ± 1.66
	R^2	0.9790	0.9712	0.9747	0.9799
	χ^2	1.025	1.301	2.420	1.239
	Freundlich				
	K_F	1.550 ± 0.378	19.16 ± 2.54	23.18 ± 3.06	26.19 ± 4.07
	$1/n$	0.493 ± 0.052	0.197 ± 0.027	0.203 ± 0.028	0.201 ± 0.034
	R^2	0.9239	0.9312	0.9332	0.9004
	χ^2	2.543	2.776	4.073	7.413

[a] $\chi^2 = (\Sigma(q_{e,exp} - q_{e,cal})^2/q_{e,cal})$, $q_{e,exp}$ and $q_{e,cal}$ are the experimental value and calculated value according the model, respectively.

and MG ions adsorbed under equilibrium conditions. It is seen that the values of q_e for NRH and MRH were the smallest at the initial pH 2.0. The lower uptake capacities of dyes at low pH are probably due to the presence of excess H^+ ions holding the sorption sites on NRH or MRH. For MB or MG basic dye, it will be positively charged in solution. As the pH of the dye solution becomes higher, the association of dye cations on the solid will take place more easily, resulting in an increase in adsorption.

For NRH, its main functional group is the hydroxyl group. Along with an increase of the pH value, the concentration of H^+ ions that compete with the dye cations for sorption sites decreased. The uptake of dyes adsorbed on NRH gradually increased as the initial pH was increased. For MRH, its practical functional group is the carboxyl group. When the pH was low, the presence of excess H^+ ions could restrain the ionization of the carboxyl group, so the nonionic form of the carboxyl group, −COOH, was present. The adsorption capacity of the dyes was small because of the absence of electrostatic interaction. When the pH was high, the carboxyl group is turned into $-COO^-$, and the adsorption capacity of the dye ions increases. The values of q_e increased as the initial pH increased from (1 to 7); they changed insignificantly beyond pH 7. From Figure 2, it can be seen that the uptake of MB and MG by MRH was much higher compared to NRH. For example, the adsorption capacity for MB was found to be 17.66 $mg\cdot g^{-1}$ for NRH and 52.31 $mg\cdot g^{-1}$ for MRH at pH 7, respectively. It is indicated that the carboxyl groups on the surface of the MRH were primarily responsible for the sorption of dyes. Similar results have been reported by Han et al.[8,22]

3.3. Effect of KCl and $CaCl_2$ Concentration on Adsorption. Dye-laden wastewaters released from different industries contain different amounts of various salts. The presence of these salts leads to a high ionic strength in the system which may significantly affect the performance of the adsorption process. From Figure 3, it can be seen that the existence of KCl and $CaCl_2$ in solution affected the equilibrium adsorption of MB and MG onto MRH. Thus, an increase in the concentration of both salts resulted in a decrease in the values of q_e. This indicated that the adsorption efficiency of the adsorbent decreased as the KCl and $CaCl_2$ concentration increased in the dye solution, which may be attributed to the competitive effect between dye ions and salt cations for the sites available for sorption. As the Ca^{2+} ions makes a greater contribution to the ionic strength as a result of increased positive charge relative to K^+, the effect of the Ca^{2+} ion on adsorption is greater than that of K^+ ion adsorption at the same mole concentration.[11]

3.4. Adsorption Equilibrium Study. The effect of the initial dye concentration on adsorption onto NRH or MRH was investigated over the range of (20 to 450) $mg\cdot L^{-1}$. Figure 4 shows the equilibrium quantity at different equilibrium dye concentrations.

From Figure 4, the values of q_e increased with increasing C_e. The dye concentration provides the necessary driving force to overcome the resistances to the mass transfer of MB and MG between the aqueous and the solid phases.[22] Increasing values of C_e also increase the interaction between dyes and adsorbents, leading to an increase in the adsorption uptake of MB or MG.

The bigger adsorptive capacity of dyes was also observed in the higher temperature range. This is not unexpected since increasing temperature would lead to higher diffusion rates accompanied by decreasing viscosity and density of the solute, all of which enhance the extent of adsorption. The observed increase in the magnitude of the equilibrium adsorption with increasing temperature also indicated that the adsorption of dye ions onto MRH was endothermic in nature.

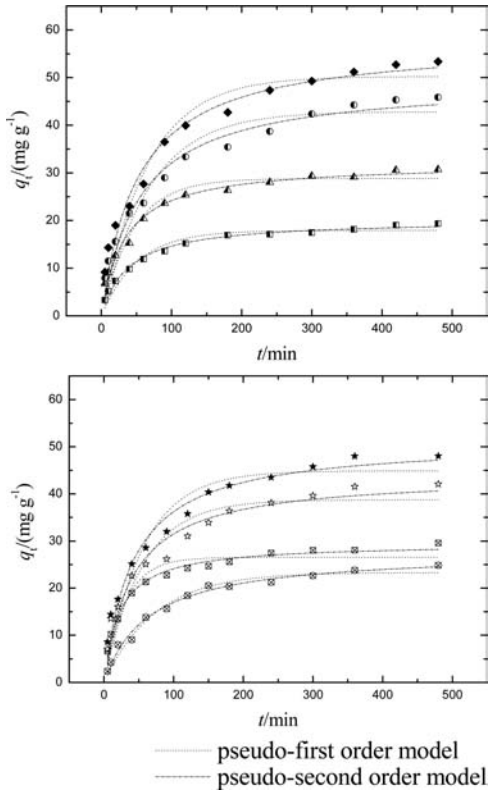

Figure 5. Effect of contact time on adsorption (NRH or MRH dosage 3 g·L^{-1}, 293 K). ◧, MB (200 mg·L^{-1}, NRH); ◭, MB (100 mg·L^{-1}); ◐, MB (150 mg·L^{-1}); ♦, MB (100 mg·L^{-1}); ⊗, MG (200 mg·L^{-1}, NRH); □ with ×, MG (100 mg·L^{-1}); ☆, MG (150 mg·L^{-1}); ★, MG (100 mg·L^{-1}).

3.5. Adsorption Isotherms of Adsorption. To optimize the design of an adsorption system for the removal of adsorbate, it is important to establish the most appropriate correlation for the equilibrium data. In the present study, the Langmuir and Freundlich isotherm models have been used to describe the adsorption equilibrium.

The Langmuir adsorption isotherm has been successfully applied to many pollutant adsorption processes and has been the most widely used sorption isotherm for the sorption of a solute from a liquid solution.[23] The common form of the Langmuir isotherm is:

$$q_e = \frac{q_{max} K_L C_e}{1 + K_L C_e} \quad (2)$$

where q_m is the q_e for a complete monolayer (mg·g^{-1}), a constant related to adsorption capacity; and K_L is a constant related to the affinity of the binding sites and energy of adsorption (L·mg^{-1}).

The Freundlich isotherm is an empirical equation describing adsorption onto a heterogeneous surface. The Freundlich isotherm is commonly presented as:[24]

$$q_e = K_F C_e^{1/n} \quad (3)$$

where K_F and $1/n$ are the Freundlich constants related to the adsorption capacity and adsorption intensity of the adsorbent, respectively.

All of the respective parameters for the isotherm equations, the determined coefficients (R^2), and the values of χ^2 are listed in Table 1, respectively. Figure 4 also shows the experimental equilibrium data and the fitted equilibrium curves obtained from the application of various isotherm models at different temperatures.

From Table 1, the values of q_m, K_L, and K_F increased with temperature for MB and MG adsorption. The obtained values of $1/n$ ($0.1 < 1/n < 1$) indicated a higher adsorption ability of the dyes at all temperatures studied. From values of R^2 and χ^2, it can be seen that the Langmuir isotherm exhibited a little better fit to the MG adsorption data by both adsorbents, while the Freundlich isotherm seemed to agree better with the MB adsorption. A comparison of experimental points and fitted curves in Figure 4 reinforced this result.

The maximal equilibrium quantity of MB and MG from the Langmuir model on MRH was (53.21 and 54.02) mg·g^{-1} at 293 K, respectively. Comparing with MRH, NRH has a small adsorption capacity of dyes. The adsorption capacities (q_m) of NRH for MB and MG were (19.77 and 28.00) mg·g^{-1} at 293 K, respectively. So the adsorption capacity of rice husk was improved by chemical modification.

3.6. Effect of Initial Concentrations and Adsorption Kinetics. The rate of MB and MG adsorption on MRH was determined as a function of the initial dye concentration. The uptake of MB and MG for three initial dye concentrations at different contact times is shown in Figure 5.

The results showed that the adsorption of MB and MG onto MRH increased with increasing contact time at different initial dye concentrations. The kinetics of adsorption of MB and MG consisted of two phases: an initial rapid phase where adsorption was fast and contributed significantly to equilibrium uptake and a slower second phase whose contribution to the total dye adsorption was relatively small. It was also seen that the equilibrium time occurred relatively early in the solution containing lower dye concentrations. Furthermore, the adsorption amount increased with an increase in initial dye concentration. The adsorption capacity of MRH for MB was (30.71, 45.87, and 53.37) mg·g^{-1} and for MG was (29.58, 42.07, and 48.04) mg·g^{-1} with three levels of concentration, respectively. The reason was that a higher initial concentration enhanced the driving force between the aqueous and the solid phases and increased the number of collisions between dye ions and adsorbents.[25]

From Figure 5, the adsorption capacity of NRH for MB and MG was 19.38 mg·g^{-1} and 24.85 mg·g^{-1} at the initial concentration of 200 mg·L^{-1}, respectively. The result indicated that the adsorption capacity of MRH was considerably increased compared to NRH for removing dyes. It is suggested that chemisorption is responsible for much of the dye uptake.

The kinetics for the adsorption of MB and MG onto MRH were analyzed by the application of the pseudo-first-order and the pseudo-second-order models, respectively.

The pseudo-first-order kinetic model is expressed as:[26]

$$q_t = q_e(1 - e^{-k_1 t}) \quad (4)$$

while the pseudo-second-order kinetic model is given by the following equation:[26,27]

$$q_t = \frac{k_2 q_e^2 t}{1 + k_2 q_e t} \quad (5)$$

where q_e and q_t are the amount of dyes adsorbed per unit weight of the adsorbent at equilibrium and at any time t, respectively (mg·g^{-1}), with k_1 being the pseudo-first-order rate constant

Table 2. Kinetic Parameters of MB and MG Adsorption onto NRH and MRH

$C_o/(mg \cdot L^{-1})$	200 (NRH)	100 (MRH)	150 (MRH)	200 (MRH)
		MB, Pseudo-First-Order Model		
$k_1/(min^{-1})$	0.020 ± 0.002	0.022 ± 0.003	0.015 ± 0.002	0.015 ± 0.002
$q_{e(cal)}/(mg \cdot g^{-1})$	17.92 ± 0.503	28.80 ± 0.863	42.83 ± 1.681	50.24 ± 1.792
$q_{e(exp)}/(mg \cdot g^{-1})$	19.38	30.71	45.87	53.37
R^2	0.9563	0.9427	0.9328	0.9425
χ^2	3.364	7.944	15.903	19.608
		MB, Pseudo-Second-Order Model		
$k_2/(g \cdot mg^{-1} \cdot min^{-1}) \cdot 10^{-4}$	13.0 ± 1.30	9.50 ± 1.20	3.80 ± 0.60	3.40 ± 0.50
$q_{e(cal)}/(mg \cdot g^{-1})$	20.18 ± 0.378	32.09 ± 0.744	49.33 ± 1.750	57.68 ± 1.922
R^2	0.9893	0.9802	0.9723	0.9744
χ^2	0.755	2.256	6.077	6.894
		MG, Pseudo-First-Order Model		
$k_1/(min^{-1})$	0.0137 ± 0.001	0.033 ± 0.0045	0.018 ± 0.0031	0.0181 ± 0.0026
$q_{e(cal)}/(mg \cdot g^{-1})$	23.31 ± 0.64	26.52 ± 0.76	38.74 ± 1.71	44.89 ± 1.72
$q_{e(exp)}/(mg \cdot g^{-1})$	24.85	29.58	42.07	48.04
R^2	0.9775	0.9308	0.9030	0.9289
χ^2	2.414	3.840	15.863	15.261
		MG, Pseudo-Second-Order Model		
$k_2/(g \cdot mg^{-1} \cdot min^{-1}) \cdot 10^{-4}$	5.70 ± 0.70	15.2 ± 1.40	5.80 ± 1.10	4.70 ± 0.70
$q_{e(cal)}/(mg \cdot g^{-1})$	27.77 ± 0.753	29.50 ± 0.469	43.96 ± 1.66	51.19 ± 1.59
R^2	0.9895	0.9875	0.9612	0.9747
χ^2	0.976	0.698	4.494	4.526

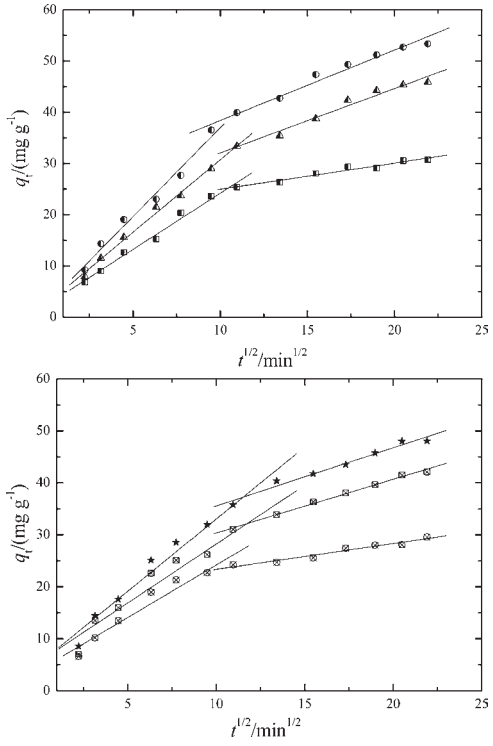

Figure 6. Intraparticle diffusion plots for MB and MG adsorption of onto MRH. ◧, MB (200 mg·L^{-1}, NRH); ◭, MB (100 mg·L^{-1}); ◐, MB (150 mg·L^{-1}); ◐, MB (100 mg·L^{-1}); ⊗, MG (200 mg·L^{-1}, NRH); □ with ×, MG (100 mg·L^{-1}); ☆, MG (150 mg·L^{-1}); ★, MG (100 mg·L^{-1}).

(min^{-1}) and k_2 being the pseudo-second-order adsorption rate constant $(g \cdot mg^{-1} \cdot min^{-1})$.

Table 2 presents the results of fitting experimental data with the pseudo-first-order and pseudo-second-order equations using nonlinear analysis. The fitted curves are also shown in Figure 5.

From Table 2, it was found that the values of q_e increased while values of k_1 and k_2 decreased when the dye concentration increased for both MB and MG adsorption. The values of R^2 (greater than 0.90) were only slightly different in the pseudo-first-order equation and pseudo-second-order equation. In addition, the calculated values of q_e obtained from both models also show good agreement with the experimental $q_{e(exp)}$ values. Hence, it was concluded that both models were capable of predicting the kinetic process measured experimentally. However, from the values of R^2 and χ^2, it was concluded that the pseudo-second-order kinetic model gave a better fit over the whole range of the adsorption process. The pseudo-second-order kinetic model assumes that chemisorption occurs,[27] and consequently the close fit observed between the model and the experimental data indicates that MB and MG adsorption onto MRH occurred in a chemical manner. Thus, the negative charge of the carboxyl group $(-COO^-)$ on the surface of MRH interacts with the positive MB and MG ions existing in solution. This suggests that the main mechanism for the adsorption behavior of MB and MG onto MRH is ion exchange.

3.7. Mechanism of Adsorption. The kinetic studies help in identifying and predicting the adsorption process, but the determination of the sorption mechanism is also important for design purposes. The pore-diffusion (intraparticle diffusion) model of Webber[28] and Boyd's equation[29] are the two most widely used models for studying the mechanism of adsorption processes.

The intraparticle diffusion model may be expressed by the equation:[28]

$$q_t = K_t t^{1/2} + C \quad (6)$$

where K_t is the intraparticle diffusion rate constant ($g \cdot mg^{-1} \cdot min^{-1/2}$) and C is a constant that provides information regarding the thickness of the boundary layer; that is, the larger the value of C the greater is the boundary layer effect.

If the plot of q_t versus $t^{1/2}$ gives a straight line, then the sorption process is controlled by intraparticle diffusion only. However, if the data exhibit multilinear plots, then two or more steps influence the sorption process. It is assumed that the external resistance to mass transfer surrounding the particles is significant only in the early stages of adsorption. This is represented by the first sharper portion. The second or third linear portion is the gradual adsorption stage with intraparticle diffusion dominating.[30]

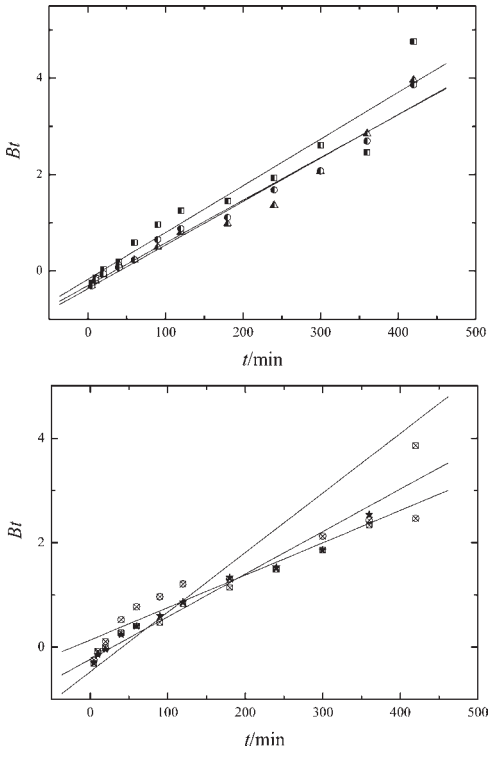

Figure 7. Plot of Bt vs t (Boyd plot). ◧, MB (100 $mg \cdot L^{-1}$); ◭, MB (150 $mg \cdot L^{-1}$); ◐, MB (200 $mg \cdot L^{-1}$); ⊗, MG (100 $mg \cdot L^{-1}$); □ with ×, MG (150 $mg \cdot L^{-1}$); ★, MG (200 $mg \cdot L^{-1}$).

Figure 6 presents the plots of q_t versus $t^{1/2}$ for MB and MG adsorption on MRH, respectively. It will be seen from the figure that the experimental data points lie on two straight intersecting lines, indicating the different stages in adsorption. For all two-linear plots in Figure 6, the regression estimates of the first linear segments had intercept values different from zero, suggesting that pore diffusion is not the step controlling the overall rate of mass transfer at the beginning of batch adsorption. Film-diffusion control may have taken place and ended in the early stages of adsorption, or maybe it is still controlling the rate of mass transfer in the time period of the first linear segment.[30] This shows that the mechanism of MB and MG adsorption onto MRH is complex and both the surface adsorption and intraparticle diffusion contribute to the actual adsorption process. It is observed in Table 3 that an increase in the initial dye concentration increases the pore diffusion rate parameters. The increase in dye concentration results in the increase of the driving force, which increases the diffusion rate of the molecular dye in the pores. It is also observed that the values of C increase with the initial concentration of the dyes, which indicates an increase in the thickness and the effect of the boundary layer.

To corroborate the actual rate-controlling steps involved in the MB and MG adsorption process, the kinetic data were further analyzed by the expression given by Boyd et al.,[29] namely,

$$F = 1 - \left(\frac{6}{\pi^2}\right)\exp(-Bt) \quad (7)$$

where B is a constant and F is the fractional attainment of

Table 4. Thermodynamic Parameters Adsorption of MB and MG by MRH

	T	ΔG	ΔH	ΔS
dye	K	$kJ \cdot mol^{-1}$	$kJ \cdot mol^{-1}$	$kJ \cdot mol^{-1} \cdot K^{-1}$
	293	−12.04		
MB	303	−12.67	6.42	0.063
	313	−13.30		
	293	−12.21		
MG	303	−13.04	12.41	0.084
	313	−13.89		

Table 3. Diffusion Coefficients for Adsorption of MB and MG on MRH at Different Initial Concentrations

C_o	C_1	C_2	K_{t1}	K_{t2}	$D_i \cdot 10^{-8}$
$mg \cdot L^{-1}$	$mg \cdot g^{-1}$	$mg \cdot g^{-1}$	$mg \cdot g^{-1} \cdot min^{-1}$	$mg \cdot g^{-1} \cdot min^{-1}$	$cm^2 \cdot s^{-1}$
			MB		
100	2.248 ± 0.748	19.828 ± 0.7939	2.192 ± 0.107	0.511 ± 0.046	1.132
150	2.413 ± 0.665	19.51 ± 1.668	2.828 ± 0.095	1.255 ± 0.096	1.135
200	2.281 ± 1.459	24.57 ± 1.453	3.469 ± 0.238	1.378 ± 0.0878	1.239
			MG		
100	3.992 ± 1.535	18.392 ± 0.870	2.018 ± 0.219	0.496 ± 0.0502	0.7939
150	5.548 ± 1.744	20.048 ± 0.673	2.266 ± 0.215	1.031 ± 0.0388	1.043
200	5.239 ± 1.484	24.346 ± 1.401	2.777 ± 0.183	1.120 ± 0.0809	1.460

Table 5. Comparison of the Adsorption Capacity for MB and MG by Various Adsorbents Reported in Literature

adsorbent	adsorption capacity ($mg \cdot g^{-1}$)	ref	adsorbent	adsorption capacity ($mg \cdot g^{-1}$)	ref
	MB			MG	
NRH	19.77	this study	NRH	28.00	this study
MRH	53.21	this study	MRH	54.02	this study
rice husk	40.6	39	rattan sawdust	62.71	48
cereal chaff	20.3	40	treated ginger waste	84.3	49
phoenix tree leaves	80.9	41	lemon peel	51.7	50
hazelnut shell	38.22	42	*Ricinus communis*	27.78	51
cotton waste	24	41	wheat bran	68.97	44
orange peel	18.6	43	rice bran	66.57	44
wheat bran	16.63	44	waste apricot	116.27	52
peanut hull	68.03	45	rubber wood sawdust	25.8−36.6	53
olive pomace	42.3	41	degreased coffee beans	55.30	54
cherry sawdust	39.68	46	maize cob powder	80.65	55
coconut husk	99	47	neem leaf powder	133.6	56

equilibrium at time t given by

$$F = \frac{q_t}{q_e} \tag{8}$$

where q_e and q_t correspond to the dye uptake $(mg \cdot g^{-1})$ at equilibrium and any time t. Equation 7 can be rearranged to:

$$Bt = -0.4997 - \ln\left(1 - \frac{q_t}{q_e}\right) \tag{9}$$

Values of Bt may be computed for each value of F and then plotted against time to obtain the Boyd plot. Such a plot is depicted in Figure 7. The linearity of these plots is employed to distinguish between external-transport-(film diffusion) and intraparticle-transport-controlled rates of adsorption. A straight line passing through the origin is shown that adsorption processes are governed by particle-diffusion mechanisms for the studied initial dye concentration; otherwise they are governed by film diffusion or external mass transport.[31]

Figure 7 shows the Boyd plots. The plots are linear in the initial period of adsorption, and all of their intercepts are not significantly different from zero, indicating that film diffusion is the rate-limiting process. In the initial adsorption period, film diffusion or chemical reaction may control the overall rate of adsorption. The presence of two pore diffusion periods in Figure 6 indicates the presence of two pore diffusion parameters, k_{t1} and k_{t2}, as shown in Table 4. The rate parameters k_{t1} and k_{t2} represented the diffusion of MB and MG in pores that have two distinct sizes (macropores and mesopores).[32] Therefore, the decrease in the value of k for macropore to mesopore diffusion was a direct consequence of the relative free path for diffusion available in each pore size. Similar results were obtained by El-Kamash et al.[33] and Wang et al.[34]

Values of B were calculated from the slope of Bt versus time plots (Figure 7). The calculated values of B for MB were (0.00969, 0.00902, and 0.00886) min^{-1} and for MG were (0.00621, 0.00816, and 0.01142) min^{-1} at initial dye concentrations of (100, 150, and 200) $mg \cdot L^{-1}$, respectively.

The values B may be employed to determine the effective diffusion coefficient (D_i) $(cm^2 \cdot s^{-1})$ of MB and MG via the relationship:[29]

$$B = \frac{\pi^2 D_i}{r^2} \tag{10}$$

where D_i is the effective diffusion coefficient for MB and MG in the adsorbent and r is the radius of the adsorbent particle assuming a spherical shape [(0.850 to 0.425) mm, 0.613 mm was chosen]. The values of D_i in Table 3 show that the relation between C_0 and the effective diffusion coefficient, D_i, has the same general trend as k_{ti}, and this trend may be related to the increasing dimerization of MB or MG with the increase of its concentration. According to Singh et al.,[35] a value of D_i of the order of (10 to 11) $cm^2 \cdot s^{-1}$ indicates that intraparticle diffusion as the rate-limiting step in the adsorption process. In this study, the values of D_i (average $(1.169 \cdot 10^{-8}$ and $1.099 \cdot 10^{-8})$ $cm^2 \cdot s^{-1}$ for MB and MG, respectively) obtained are in the order of 10^{-8} $cm^2 \cdot s^{-1}$, which is 3 orders of magnitude greater than the value quoted by Singh et al.[35] This indicates that intraparticle diffusion is not the rate-controlling step. Similar results have been reported by Kumar et al.[36] and Hameed and El-Khaiary.[37]

3.8. Adsorption Thermodynamics. Thermodynamic parameters are important in adsorption studies for a better understanding of the temperature on adsorption. The Gibbs energy change, ΔG, the standard enthalpy change, ΔH, and the standard entropy change, ΔS, were calculated via the following equation:

$$\Delta G = -RT \ln K_c' \tag{11}$$

$$\Delta G = \Delta H - T\Delta S \tag{12}$$

The apparent equilibrium constant (K_c') for the adsorption process may be defined as:

$$K_c' = \frac{C_{ad,e}}{C_e} \tag{13}$$

Using the value of K_c' obtained at the lowest smallest MB or MG concentration employed allowed the value of the change in the Gibbs energy to be calculated via eq 11.[38] The corresponding values of ΔG for the three temperatures studied in the present work are listed in Table 4. The values of the standard enthalpy

change, ΔH, and the standard entropy change, ΔS, were determined from the slope and intercept of the plot derived from eq 12.

The positive value of ΔH indicates that the adsorption process was endothermic while its magnitude supports the partial chemical nature of the process involved. The negative values of ΔG observed at the various temperatures indicate that the adsorption process was spontaneous, with the decrease in the negative value of ΔG with increasing temperature, indicating that the spontaneous nature of MB and MG adsorption was inversely proportional to the temperature. The positive value of ΔS confirms the increasing randomness at the solid−solution interface during adsorption and reflects the adsorbent for the dye.

3.9. Comparisons with Other Adsorbents. Many adsorbents for MB and MG removal, including activated carbon and various biosorbents, have been reported in the literature. The most important parameter to compare is the Langmuir q_m value since it is a measure of adsorption capacity of the adsorbent. Part of the data on MB and MG sorption capacity (values of q_m derived from the Langmuir equation) of various adsorbents, especially the low cost adsorbents, is summarized in Table 5. The adsorption capacity for MB and MG using the NRH and MRH is of the same order of magnitude or greater than that which has been found using similar adsorbents. The results indicated that the MRH can be considered a promising adsorbent for the removal of MB and MG from aqueous solutions.

AUTHOR INFORMATION

Corresponding Author

*Tel.: +86 371 67781801. Fax: +86 371 67781801. E-mail address: whzou@zzu.edu.cn; rphan67@zzu.edu.cn.

Funding Sources

This work was supported by the Education Department of Henan Province in China (No. 2010A610003) and the Henan Science and Technology Department in China (No. 102102210103).

REFERENCES

(1) Crini, G. Non-conventional low-cost adsorbents for dye removal: a review. *Bioresour. Technol.* **2006**, *97*, 1061–1085.

(2) Zollinger, H. Color chemistry-synthesis. *Properties and Application of Organic Dyes and Pigments*; VCH Publishers: New York, 1987; p 128.

(3) Robinson, T.; McMullan, G.; Marchant, R.; Nigam, P. Remediation of dyes in textile effluent: a critical review on current treatment technologies with a proposed alternative. *Bioresour. Technol.* **2001**, *77*, 247–255.

(4) Aksu, Z. Application of biosorption for the removal of organic pollutants: a review. *Process Biochem.* **2005**, *40*, 997–1026.

(5) Batzias, F. A.; Sidiras, D. K. Dye adsorption by prehydrolysed beech sawdust in batch and fixed-bed systems. *Bioresour. Technol.* **2007**, *98*, 1208–1217.

(6) Doğan, M.; Özdemir, Y.; Alkan, M. Adsorption kinetics and mechanism of cationic methyl violet and methylene blue dyes onto sepiolite. *Dyes Pigm.* **2007**, *75*, 701–713.

(7) Wang, X. S.; Zhou, Y.; Jiang, Y. Evaluation of Marine Brown Laminaria japonica Algae as a Low-cost Adsorbent for the Removal of Malachite Green Dye from Aqueous Solution. *Adsorpt. Sci. Technol.* **2009**, *27*, 537–548.

(8) Han, R. P.; Han, P.; Cai, Z. H.; Zhao, Z. H.; Tang, M. S. Kinetics and isotherms of neutral red adsorption on peanut husk. *J. Environ. Sci.* **2008**, *20*, 1035–1041.

(9) Saliba, R.; Gauthier, H.; Gauthier, R.; Petit-Ramel, M. The Use of Eucalyptus Barks for the Adsorption of Heavy Metal Ions and Dyes. *Adsorpt. Sci. Technol.* **2002**, *20*, 119–129.

(10) Bulut, Y.; Aydin, H. Kinetics and thermodynamics study of methylene blue adsorption on wheat shells. *Desalination* **2006**, *194*, 259–267.

(11) Han, R. P.; Wang, Y. F.; Han, P.; Shi, J.; Yang, J.; Lu, Y. S. Removal of methylene blue from aqueous solution by chaff in batch mode. *J. Hazard. Mater.* **2006**, *137*, 550–557.

(12) Sivaraj, R.; Namasivayam, C.; Kadirvelu, K. Orange peel as an adsorbent in the removal of acid violet 17 (acid dye) from aqueous solutions. *Waste Manage.* **2001**, *21*, 105–110.

(13) Han, R. P.; Wang, Y.; Zhao, X.; Wang, Y. F.; Xie, F. L.; Cheng, J. M.; Tang, M. S. Adsorption of methylene blue by phoenix tree leaf powder in a fixed-bed column: experiments and prediction of breakthrough curves. *Desalination* **2009**, *245*, 284–297.

(14) Gong, R. M.; Zhong, K. D.; Hu, Y.; Chen, J.; Zhu, G. P. Thermochemical esterifying citric acid onto lignocellulose for enhancing methylene blue sorption capacity of rice straw. *J. Environ. Manage.* **2008**, *88*, 875–880.

(15) Gurgel, L. V. A.; Freitas, R. P.; Gil, L. F. Adsorption of Cu(II), Cd(II), and Pb(II) from aqueous single metal solutions by sugarcane bagasse and mercerized sugarcane bagasse chemically modified with succinic anhydride. *Carbohyd. Polym.* **2008**, *74*, 922–929.

(16) Ong, S. T.; Lee, C. K.; Zainal, Z. Removal of basic and reactive dyes using ethylenediamine modified rice hull. *Bioresour. Technol.* **2007**, *98*, 2792–2799.

(17) Šćiban, M.; Klašnja, M.; Škrbić, B. Adsorption of copper ions from water by modified agricultural by-products. *Desalination* **2008**, *229*, 170–180.

(18) Vaughan, T.; Seo, C. W.; Marshall, W. E. Removal of selected metal ions from aqueous solution using modified corncobs. *Bioresour. Technol.* **2001**, *78*, 133–139.

(19) Han, R. P.; Li, Y. H.; Li, H. Q.; Wu, Y. J.; Shi, J. The elemental analysis and FT-IR comparison between MDP and casting. *Spectrosc. Spectral Anal.* **2004**, *24*, 185–186.

(20) Tarley, C. R. T.; Arruda, M. A. Z. Biosorption of heavy metals using rice milling by-products. Characterisation and application for removal of metals from aqueous effluents. *Chemosphere* **2004**, *54*, 987–995.

(21) Crini, G.; Peindy, H. N.; Gimbert, F.; Robert, C. Removal of C. I. Basic Green 4 (malachite green) from aqueous solutions by adsorption using cyclodextrinbased adsorbent: kinetic and equilibrium studies. *Sep. Purif. Technol.* **2007**, *53*, 97–110.

(22) Han, R. P.; Zhang, L. J.; Song, C.; Zhang, M. M.; Zhu, H. M.; Zhang, L. J. Characterization of modified wheat straw, kinetic and equilibrium study about copper ion and methylene blue adsorption in batch mode. *Carbohyd. Polym.* **2010**, *79*, 1140–1149.

(23) Langmuir, I. The constitution and fundamental properties of solids and liquids. *J. Am. Chem. Soc.* **1916**, *38*, 2221–2295.

(24) Freundlich, H. M. F. Uber die adsorption in lasungen. *J. Phys. Chem.* **1906**, *57*, 385–470.

(25) Ozer, A.; Akkaya, G. The removal of Acid Red 274 from wastewater: combined biosorption and biocoagulation with *Spirogyra rhizopus*. *Dyes Pig.* **2006**, *71*, 83–89.

(26) Ho, Y. S.; Ng, J. C. Y.; McKay, G. Kinetics of pollutant sorption by biosorbents: Review. *Sep. Purif. Methods* **2000**, *29*, 189–232.

(27) Ho, Y. S.; McKay, G. Pseudo-second-order model for sorption process. *Process Biochem.* **1999**, *34*, 451–465.

(28) Weber, W. J., Jr.; Morris, J. C. Kinetics of adsorption on carbon from solution. *J. Sanit. Eng. Div., Proc. Am. Soc. Civil Eng.* **1963**, *89*, 31–59.

(29) Boyd, G. E.; Adamson, A. W.; Myers, L. S., Jr. The exchange adsorption of ions from aqueous solutions by organic zeolites. II: Kinetics. *J. Am. Chem. Soc.* **1947**, *69*, 2836–2848.

(30) Srivastava, V. C.; Swamy, M. M.; Mall, I. D.; Prasad, B.; Mishra, I. M. Adsorptive removal of phenol by bagasse fly ash and activated carbon: Equilibrium, kinetics and thermodynamics. *Colloids Surf., A* **2006**, *272*, 89–104.

(31) Mohan, D.; Singh, K. P. Single- and multi-component adsorption of cadmium and zinc using activated carbon derived from bagasse-an agricultural waste. *Water Res.* **2002**, *36*, 2304–2318.
(32) Allen, S. J.; McKay, G.; Khader, K. Y. H. Intraparticle diffusion of a basic dye during adsorption onto sphagnum peat. *Environ. Pollut.* **1989**, *56*, 39–50.
(33) El-Kamash, A. M.; Zaki, A. A.; Abed-El-Geleel, M. Modeling batch kinetics and thermodynamics of zinc and cadmium removal from waste solutions using synthetic zeolite A. *J. Hazard. Mater.* **2005**, *127*, 211–220.
(34) Wang, X. S.; Qin, Y.; Li, Z. F. Biosorption of zinc from aqueous solutions by rice bran: kinetics and equilibrium studies. *Sep. Sci. Technol.* **2006**, *41*, 747–756.
(35) Singh, K. K.; Rastogi, R.; Hasan, S. H. Removal of Cr(VI) f rom wastewater using rice bran. *J. Colloid Interface Sci.* **2005**, *290*, 61–68.
(36) Kumar, K. V.; Ramamurthi, V.; Sivanesan, S. Modeling the mechanism involved during the sorption of methylene blue onto fly ash. *J. Colloid Interface Sci.* **2005**, *284*, 14–21.
(37) Hameed, B. H.; El-Khaiary, M. I. Equilibrium, kinetics and mechanism of malachite green adsorption on activated carbon prepared from bamboo by K_2CO_3 activation and subsequent gasification with CO_2. *J. Hazard. Mater.* **2008**, *157*, 344–351.
(38) Catts, J. G.; Langmuir, D. Adsorption of Cu, Pb, and Zn by d-MnO_2: Applicability of the side binding-surface complexation model. *Appl. Geochem.* **1986**, *1*, 255–264.
(39) Vadivelan, V.; Kumar, K. V. Equilibrium, kinetics, mechanism, and process design for the sorption of methylene blue onto rice husk. *J. Colloid Interface Sci.* **2005**, *286*, 90–100.
(40) Han, R. P.; Wang, Y. F.; Han, P.; Shi, J.; Yang, J.; Lu, Y. S. Removal of methylene blue from aqueous solution by chaff in batch mode. *J. Hazard. Mater.* **2006**, *137*, 550–557.
(41) Rafatullah, M.; Sulaiman, O.; Hashim, R.; Ahmad, A. Adsorption of methylene blue on low-cost adsorbents: A review. *J. Hazard. Mater.* **2010**, *177*, 70–80.
(42) Dogan, M.; Abak, H.; Alkan, M. Biosorption of methylene blue from aqueous solutions by hazelnut shells: equilibrium, parameters and isotherms. *Water, Air, Soil Pollut.* **2008**, *192*, 141–153.
(43) Annadurai, G.; Juang, R.; Lee, D. Use of cellulose-based wastes for adsorption of dyes from aqueous solutions. *J. Hazard. Mater.* **2002**, *B92*, 263–274.
(44) Wang, X. S.; Zhou, Y.; Jiang, Y.; Sun, C. The removal of basic dyes from aqueous solutions using agricultural by-products. *J. Hazard. Mater.* **2008**, *157*, 374–385.
(45) Gong, R. M.; Li, M.; Yang, C.; Sun, Y.; Chen, J. Removal of cationic dyes from aqueous solution by adsorption on peanut hull. *J. Hazard. Mater.* **2005**, *B121*, 247–250.
(46) Lata, H.; Garg, V. K.; Gupta, R. K. Removal of a basic dye from aqueous solution by adsorption using *Parthenium hysterophorus*: an agricultural waste. *Dyes Pigm.* **2007**, *74*, 653–658.
(47) Low, K. S.; Lee, C. K. The removal of cationic dyes using coconut husk as an absorbent. *Pertanika* **1990**, *13*, 221–228.
(48) Hameed, B. H.; El-Khaiary, M. I. Malachite green adsorption by rattan sawdust: Isotherm, kinetic and mechanism modeling. *J. Hazard. Mater.* **2008**, *159*, 574–579.
(49) Ahmad, R.; Kumar, R. Adsorption studies of hazardous malachite green onto treated ginger waste. *J. Environ. Manage.* **2010**, *91*, 1032–1038.
(50) Kumar, K. V. Optimum sorption isotherm by linear and non-linear methods for malachite green onto lemon peel. *Dyes Pigm.* **2007**, *74*, 595–597.
(51) Santhi, T.; Manonmani, S.; Smitha, T. Removal of malachite green from aqueous solution by activated carbon prepared from the epicarp of *Ricinus communis* by adsorption. *J. Hazard. Mater.* **2010**, *179*, 178–186.
(52) Başar, C. A. Applicability of the various adsorption models of three dyes adsorption onto activated carbon prepared apricot. *J. Hazard. Mater.* **2006**, *B135*, 232–241.
(53) Kumar, K. V.; Sivanesan, S. Isotherms for Malachite Green onto rubber wood (*Hevea brasiliensis*) sawdust: comparison of linear and non-linear methods. *Dyes Pigm.* **2007**, *72*, 124–129.
(54) Baek, M.-H.; Ijagbemi, C. O.; Se-Jin, O.; Kim, D.-S. Removal of Malachite Green from aqueous solution using degreased coffee bean. *J. Hazard. Mater.* **2010**, *176*, 820–828.
(55) Sonawane, G. H.; Shrivastava, V. S. Kinetics of decolourization of malachite green from aqueous medium by maize cob (*Zea maize*): An agricultural solid waste. *Desalination* **2009**, *247*, 430–441.
(56) Bhattacharyya, K. G.; Sharma, A. Adsorption characteristics of the dye, Brilliant Green, on Neem leaf powder. *Dyes Pigm.* **2003**, *57*, 211–222.